The Y39A Mutation of HK022 Nun Disrupts a *boxB* Interaction but Preserves Termination Activity†

Björn M. Burmann,‡ Augusto Uc-Mass,§ Kristian Schweimer,‡ Max E. Gottesman,§ and Paul Rösch*,‡

Department of Biopolymers and Research Center for Bio-Macromolecules, Universität Bayreuth, Universitätsstrasse 30, 95447 Bayreuth, Germany, and Department of Microbiology and Institute of Cancer Research, Columbia University Medical Center, New York, New York 10032

Received March 14, 2008; Revised Manuscript Received May 7, 2008

ABSTRACT: Coliphage HK022 Nun protein targets phage λ *nut boxB* RNA and acts as a transcriptional terminator, counteracting the phage λ N protein, a suppressor of transcription termination. Both Nun and N protein interact directly with RNA polymerase, and Nun competes with N protein for *boxB* binding and prevents superinfection of *Escherichia coli* HK022 lysogens by λ. Interaction of Trp18 of λ N and A7 of *boxB* RNA in the N−*boxB* complex is essential for efficient antitermination. We found that the corresponding Nun mutation, Nun Y39A, disrupts the interaction between the aromatic ring of Y39 and A7, but the mutant retains in vivo termination activity. Stabilization of the complex by interaction of A7 with an aromatic amino acid is thus less important for Nun activity than it is for N activity. Structural investigations show similar binding of mutant and wild-type (wt) Nun protein to *boxB* RNA. The dissociation constants of the wt Nun(20−44)−*boxB* and mutant Nun(20−44)−*boxB* complex as well as the structures of the *boxB* RNA in both complexes are identical.

Coliphage HK022 Nun protein blocks superinfection of HK022 lysogens by the related phage λ (*1, 2*). Both phage λ N protein and HK022 Nun protein interact with the *Escherichia coli* transcription elongation complex (TEC)[1] which includes RNA polymerase (RNAP) and *E. coli* proteins NusA, NusB, NusE (S10 ribosomal subunit), and NusG (*3, 4*). The consequence of this interaction is opposite for the two proteins: λ N suppresses transcription termination (*1, 5*), whereas HK022 Nun promotes it (*6*). Nun attaches to the *boxB* RNA sequence, a 15-mer hairpin structure with a purine-rich pentaloop (*7, 8*), of two *cis*-acting elements, λ *nutR* and λ *nutL*, of the λ nascent transcript. The sequence of *nutL boxB* differs from the sequence of *nutR boxB* by a single G-to-A substitution. The 107-amino acid protein Nun contains an amino-terminal domain with an as-yet-unknown function, followed by an arginine-rich motif (ARM) that binds *boxB* RNA (*9*), and a C-terminal putative DNA/RNAP interaction domain (*10*).

Both λ N and HK022 Nun bind to *boxB* RNA with similar affinities in the low nanomolar range via their ARM (λ N ARM, QTRRRERRAEKQ; HK022 Nun ARM, RDRRRIARWEKR) (*11–13*). Similar to the N(1−36) peptide, the Nun(20−44) peptide containing the ARM folds into a bent α-helix upon complex formation, and *boxB* RNA attains a GNRA tetraloop formation with an extruded A7 (*12–14*). S24 and R28 intercalate with bases of the 5′ stem, and it was proposed that the structure is further stabilized by π−π interaction between Y39 and *boxB* A7 which is observed in the λ N−*boxB* RNA complex W18−*boxB* A7 interaction (*12–14*). Our recent studies, however, show this amino acid−base stacking to be required neither for binding nor for correct RNA folding into the canonical GNRA tetraloop conformation that is attained by the pentaloop on λ N−HK022 Nun ARM binding. For wild-type (wt) λ N, Xia et al. (*15, 16*) observed that the stacked conformation is only transiently populated and an equilibrium between the stacked and open conformation on the picosecond time scale was observed. However, the requirement for an aromatic amino acid at this position for efficient antitermination *in vivo* and *in vitro* was determined (*15, 17, 18*). The Nun Y39A mutant shows termination activity *in vivo* despite the lack of the Nun Y39−*boxB* A7 interaction, in striking difference to λ N which requires the W18−*boxB* A7 base interaction for full activity. Combining fluorescence equilibrium titrations, NMR, and molecular dynamics (MD) simulations, we were able to relate structural features of the protein with its physiological termination activity in vivo.

MATERIALS AND METHODS

Sample Preparation. Unlabeled 15-nucleotide *nutR boxB* RNA was synthesized by *in vitro* transcription using T7 polymerase, a synthetic DNA template (5′-GCCCTTTTTCAGGGCTATAGTGAGTCGTATTA-3′, Biomers, Ulm, Ger-

† This project was supported by a grant to P.R. from the Deutsche Forschungsgemeinschaft DFG (Ro617/16-1). M.E.G. is supported by NIH Grant GM37219.

* To whom correspondence should be addressed: Research Center for Bio-Macromolecules, Universität Bayreuth, Universitätsstr. 30, 95440 Bayreuth, Germany. Phone: +49 921 553540. Fax: +49 921 16490459. E-mail: roesch@unibt.de.

‡ Universität Bayreuth.

§ Columbia University Medical Center.

[1] Abbreviations: ARM, arginine-rich motif; *nut*, N utilization site; Nus, N utilization substance; MD, molecular dynamics; COSY, correlated spectroscopy; EOP, efficiency of plating; NOESY, nuclear Overhauser enhancement spectroscopy; RNAP, RNA polymerase; rmsd, root-mean-square deviation; TEC, transcription elongation complex; TOCSY, total coherence spectroscopy.

10.1021/bi8004347 CCC: $40.75
Published on Web 06/19/2008

many), and unlabeled nucleotide triphosphates. RNA was purified as described previously (*13*). Freeze-dried RNA was resuspended in NMR buffer [50 mM potassium phosphate and 40 mM NaCl (pH 6.4)], heated for 5 min at 95 °C, cooled for refolding, dialyzed against water, and freeze-dried for storage. This RNA was directly dissolved in NMR buffer for experiments. 3′-(6-Fam)-labeled *nutR boxB* for fluorescence measurements was obtained from Biomers and used according to the manufacturer's instructions.

Nun(20−44) (RGLTSRDRRRIARWEKRIAYALKNG) and Nun(20−44) Y39A were purchased from PANATecs (Tübingen, Germany), dialyzed against water for desalting, and freeze-dried. Nun(20−44) Y39A−*nutR boxB* RNA samples were generated by adding small volumes of a concentrated RNA solution to the peptide. For further concentration, the complex was freeze-dried and resuspended in a H_2O/D_2O mixture. Part of the peptide aggregated upon binding to the RNA as observed for wt Nun (*12*), and concentrations were thus limited to less than 500 μM.

Fluorescence Measurements. Extrinsic fluorescence measurements with 3′-6-carboxyfluorescein (6-Fam)-labeled *nutR boxB* RNA were performed in NMR buffer in a volume of 1 mL using a 10 mm × 4 mm quartz cuvette (Hellma, Müllheim, Germany) with an L-format Jobin-Yvon (Edison, NJ) Horiba Fluoromax fluorimeter. The excitation wavelength was 492 nm, and the emission intensity was detected at 516 nm applying a 500 nm cutoff filter. The slit widths were 9 and 7 nm for excitation and emission, respectively, and all titration measurements were taken at 25 °C with the fluorescence-labeled RNA at 50 pM. Stock peptide solutions contained 1 μM Nun and Nun(20−44) Y39A. Following sample equilibration, 100 data points with an integration time of 0.1 s were collected for each titration step.

Data Fitting. Data were fitted to a two-state binding equation to determine the equilibrium dissociation constant (K_d) using standard software:

$$F = F_{min} - (F_{max} - F_{min})\left[(K_d + [P]_0 + [RNA]_0)\frac{\sqrt{(K_d+[P]_0+[RNA]_0)^2-4[P]_0[RNA]_0}}{2[RNA]_0}\right] \quad (1)$$

where F is the fluorescence intensity, F_{max} and F_{min} are the signal intensities of the bound and unbound form, respectively, and $[P]_0$ and $[RNA]_0$ are the total protein and RNA concentration, respectively.

For displacement experiments, labeled RNA and Nun peptide at 10 nM were used, and the absolute concentrations were significantly higher than the determined dissociation constant. Therefore, the titration starts at a 1:1 ratio of Nun to labeled RNA with negligible concentrations of free protein and RNA in solution, and the displacement titration was evaluated with (*19*)

$$F = F_{max} - (F_{max} - F_{min})\left[K_r([P]_0 + [RNA]_0)\frac{\sqrt{(K_r[P]_0+K_r[RNA]_0)^2-4(K_r-1)K_r[P]_0[RNA]_0}}{[P]_0(K_r-1)}\right] \quad (2)$$

where F_{max} is the relative fluorescence intensity at the beginning of the titration, F_{min} is the intensity under saturating conditions of the unlabeled RNA, and K_r is the relative affinity of the unlabeled and labeled RNA ($K_r = K_1/K_2$, where K_1 is the dissociation constant of labeled RNA and K_2 is the dissociation constant of unlabeled RNA).

NMR Measurements. All NMR experiments were recorded at either 298 K (one-dimensional experiments) or 303 K (two-dimensional experiments) on Bruker DRX 600 MHz and AV 700 MHz spectrometers with triple-resonance probes equipped with pulsed field gradient capabilities. For resonance assignments, correlated spectroscopy (COSY), total coherence spectroscopy (TOCSY), and nuclear Overhauser enhancement spectroscopy (NOESY) experiments were performed using standard techniques for recording and water suppression (*20*). All NMR data were analyzed with NMRView version 5.2.2 (*21*) and in house routines.

All our experimental data clearly indicated that the fold of the *boxB* RNA in the Nun Y39A complex is identical to the fold of the wt Nun−*boxB* [Protein Data Bank (PDB) entry 1HJI] complex and thus virtually identical to the fold of *boxB* in the λ N(1−36)−*boxB* (PDB entry 1QFQ) complex (*12, 13*), rendering it plausible to use this *boxB* RNA structure as a fixed template for all MD calculations.

All structure calculations were performed using a modified ab initio simulated annealing protocol with an extended version of Xplor-NIH 1.2.1 (*22, 23*). The calculation strategy as described previously (*24*) included floating assignment of prochiral groups (*25*), a conformational database potential term (*26*), and a reduced presentation for nonbonded interactions for part of the calculation (*24*). The protocol was identical to that used previously (*11*). For analysis, PROCHECK-NMR (*27*) was used, and for graphical presentations, PyMol (*28*) was used.

In Vivo Assays. Plasmid *pTrc99* (Amersham Bioscience) is a ColE1 plasmid encoding ampicillin resistance. Plasmid *pTrc-Nun* is *pTrc99* carrying *nun* under *tac* promoter control (Gottesman laboratory collection), resulting in a general test system for Nun activity. Plasmid *pTrc-Nun Y39A* was constructed by introducing a mutation into codon 39 of the *nun* gene cloned in *pTrc-Nun* using the Quickchange site-directed mutagenesis kit (Stratagene). The mutation substitutes a tyrosine residue at position 39 for alanine. The following primers were used: Y39Af, TGG GAA AAA AGG ATA GCA GCC GCA TTA AAA AAC GGT GTG; and Y39Ar, CAC ACC GTT TTT TAA TGC GGC TGC TAT CCT TTT TTC CCA.

Strains. Strains used in this study were *E. coli* W3102 (N99, NIH collection) and its derivatives *N99lacZXA21* (Gottesman laboratory collection), N99 *λcI857*-pL-*nutL-N:lacZ* (*29*), and *N99lacZXA21 λcI857-pR-cro-nutR-cII:lacZ* (from N. Costantino and D. Court).

Efficiency of λ Plating (EOP). Fresh overnight cultures of N99 transformed with pTrc99, pTrc-Nun, and pTrc-Nun Y39A were poured atop agar on LB plates. EOPs were determined by spotting dilutions of λ and incubation overnight at 37 °C.

Termination Efficiency. Log phase cultures of strains N99 *lacZXA21*, N99 *λcI857-pL-nutL-N:lacZ*, and N99 *lacZXA21 λcI857-pR-cro-nutR-cII:lacZ* transformed with pTrc99, pTrc-Nun, and pTrc-Nun Y39A were heated from 32 to 42 °C and incubated for 1 h. Samples were assayed for β-galactosidase activity as described previously (*30*). The shift to 42 °C inactivates the *λcI857* repressor, permitting transcription from the λpL and λpR promoters. The percent of readthrough was calculated as described by Kim et al. (*31*).

MD Simulations. The Amber 9 program package (*32*) and the *ff03* force field (*33, 34*) were used for the simulations of

Table 1: Nun Y39A Is as Efficient as wt Nun for λ Exclusion and Transcription Termination[a]

plasmid	read-through (%)		
	EOP[b]	*pL-nutL-N:lacZ*[c]	*pR-cro-nutR-tR1-cII:lacZ*[c]
pTrc99	1	100	100
pTrc-Nun	10^{-6}	1	3
pTrc-Nun Y39A	10^{-6}	9	7

[a] Induction is for 1 h at 42 °C. λ-Galactosidase assays are as described previously (*29*). All data are averages of two independent experiments. [b] Strain W3102 transformed with the indicated plasmids was spotted with λ at 37 °C. [c] Nun sensitive fusions are controlled by the temperature sensitive cI857 repressor.

the wt Nun(20−44)−*nutR boxB* and Nun(20−44) Y39A−*nutR boxB* complexes. The simulation for the wt complex was based on the NMR structure of the complex (PDB entry 1HJI). For the in silico mutation of the peptide, the Loopy program from the Jackal suite (http://wiki.c2b2.columbia.edu/honiglab_public/index.php/Software:Jackal) was used to alter the wt PDB entry and to provide a correct insertion of A39.

The RNA−peptide complexes were solvated in a TIP3P water box (*35*) with dimensions of 60 Å × 60 Å × 60 Å, and sodium counterions were added *in silico* for neutralization of the system. Calculations were performed at 298 K and an external pressure of 1 atm. Under these conditions, the systems were minimized and equilibrated using SANDER. Initially, the whole system was minimized for 1000 steps, and the water molecules and counterions were relaxed around the fixed solute with a 100 ps MD run. MD production runs 20 ns in duration were then performed for both systems. The MD data were analyzed by using PTRAJ. Root-mean-square deviation (rmsd) calculations of the atomic coordinates were referenced to the first calculated structure.

RESULTS AND DISCUSSION

Nun Y39A Is Active in Vivo. Phage HK022 Nun protein excludes superinfection of λ by terminating the λpL and λpR early transcripts just distal from the *nut* sites. We tested the in vivo activity of Nun Y39A by determining the efficiency of plating (EOP) of λ on a lawn of *E. coli* carrying plasmid *pTrc-Nun Y39A*. We found that λ forms plaques on cells expressing wild-type Nun or Nun Y39A with very low efficiency ($<10^{-6}$) compared to the control strain carrying empty vector (in Table 1, compare rows 2 and 3 with row 1). These results show that Nun Y39A is as efficient as wt Nun at excluding λ. We then tested Nun Y39A for termination in two λ*nut-lacZ* fusions (see Materials and Methods). The level of β-galactosidase activity provides a quantitative measure of Nun termination efficiency at *nutL* and *nutR*. Our data show that the percent read-through with Nun Y39A is only slightly higher than with wt Nun protein (in Table 1, compare columns 2 and 3). In conclusion, our data show no significant differences between the activities of Nun Y39A and wt Nun, suggesting that the binding of Nun Y39A to *boxB* should be equivalent to that of wt Nun as far as termination activity is concerned.

Mutation of equivalent amino acids affected HK022 Nun and λ N activity to a different degree (Table 2) (*17, 18*). Amino acids whose variation in λ N led to a loss of RNA binding activity according to gel mobility shift assays caused only a minor loss of termination activity of HK022 Nun, with the most notable effect caused by Nun mutations R25A, R27A, and R32A (71, 84, and 83% termination efficiency, respectively) in the contact region of Nun and the RNA stem (*12*). λ N activity is thus more critically dependent on key amino acid variations than Nun activity.

Table 2: Effect of Nun Mutations on Antitermination Activity

	pL-cro-nutR-lacZ[a]	λ exclusion[b]	λ nin exclusion[b,c]
Nun$^+$	97	+	+
vector	0	−	−
R25A	71	+	+
R27A	84	+	+
A31L	93	+	+
R32A	83	+	+
K35A	93	+	+
R36A	91	+	+
Y39A	93	+	+
N43A	96	+	+

[a] Values represent the percent termination based on β-galactosidase assays. [b] Exclusion was determined as described in Materials and Methods. [c] λ *nin* is deleted for terminators between λ genes P and Q and does not require N for growth. Thus, the Nun mutants are not merely competing with λ N for *boxB* RNA binding but are actively terminating transcription.

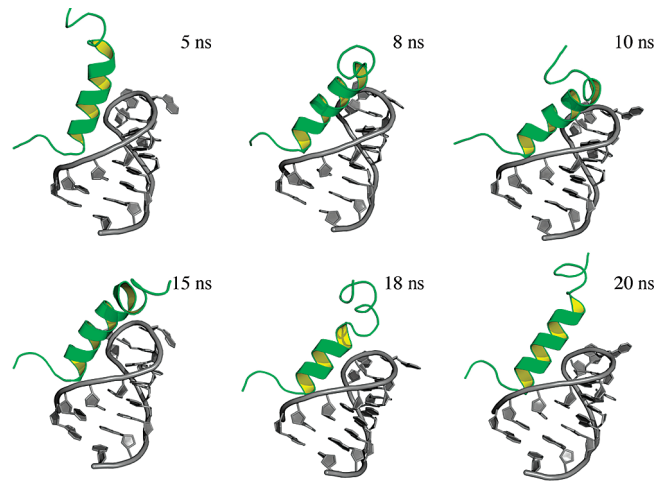

FIGURE 1: Snapshots taken from the MD simulation of the Nun Y39A−RNA complex showing a high degree of flexibility for amino acids 31−44 of the Nun Y39A peptide (green). Typical features of the RNA (gray) are the helical turn in the stem region and the GNRA tetraloop with extruded base A9. The RNA is slightly flexible in the loop region.

The Carboxy Terminus of Nun(20−44) Y39A Is Highly Flexible in MD Simulations. MD simulations of the wt Nun(20−44)−*boxB* RNA and Nun(20−44) Y39A−*boxB* RNA complexes showed that the conformation of Nun(20−44) Y39A in the complex is defined well only from S24 to I30, whereas the wt complex is stable and defined well over the whole simulation time of 20 ns. The carboxy-terminal helix of the peptide, R32−G44, possessed a high degree of flexibility without preferential orientation but retained helical structure (Figure 1). Other indicators of flexibility of the peptide in the complex are the rmsd values of both simulations (Figure 2A), indicating the mutant peptide in the complex to be more flexible than the wt peptide. The variation of the distance between Y39 and RNA A7 for the wt complex compared to the mutant A39 and RNA A7 distance rules out hydrophobic interaction between the three alanines (38−40) and RNA A7 as the distance between Hβ atoms of these alanines and RNA A7 H8 is greater than 10 Å.

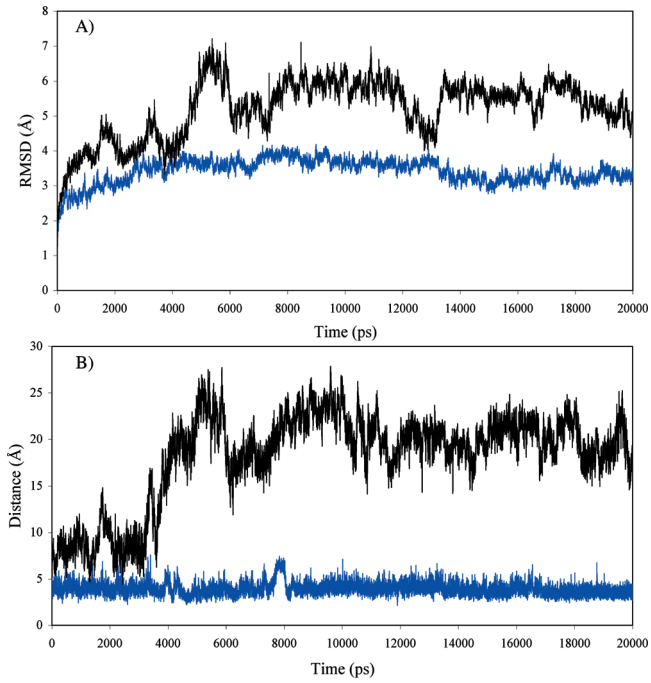

FIGURE 2: (A) rmsd values for Nun (blue) and Nun Y39A (black) as a function of simulation time referenced to the first calculated structure. (B) Distance between Tyr39 Hδ1 and A7 H8 for Nun (blue) and Ala39 Hβ2 and A7 H8 for NunY39A (black) as a function of simulation time.

Surprisingly, the structure of the RNA remains stable in both simulations, retaining the helical turn in the stem region as well as the GNRA tetraloop with A9 extruded. Thus, the equilibrium between folded and unfolded RNA is shifted toward the folded species by binding of either peptide, although the RNA loop region is more flexible in the complex with the mutant peptide.

NunY39A Forms a Well-Defined Complex with the boxB RNA. One-dimensional NMR spectra show directly the binding of the peptide to the RNA in the imino proton region. For free RNA, only the imino proton resonances of G12, G13, and G14 were observed. Upon addition of Nun(20−44) Y39A, these resonances shifted, and the imino proton resonances of U5 and G6 as well as the indole NH resonance of W33 could be detected (compare Figure 3B to wt in Figure 3A). This increase in number and the change in the position of these resonances are typical signs of the stabilization of *boxB* by these peptides. Both Nun complexes resulted in the same number and pattern of imino proton signals between 10 and 14 ppm, indicating that the mutant peptide induces RNA stem structure similar to the structure induced by the wt peptide, and appearance of the G6 resonance suggests the formation of the sheared G6-A10 base pair that leads to the formation of the GNRA tetraloop. The emergence of the U5 imino resonance in either spectrum relates to the stabilization of the apical U5-A11 base pair. These results indicate that the binding of the mutant peptide to the *boxB* RNA follows the same general pattern in the stem region as the wt peptide.

The wt Nun−boxB Complex Is Marginally More Stable Than the Nun Y39A−boxB Complex. To determine the contribution of the tyrosine base stacking interaction to complex stability, the K_d values were determined for the mutant and wt peptide with fluorescence titrations at 516 nm employing 3′-(6-Fam)-labeled *nutR boxB* RNA. K_d values were 2.4 ± 0.1 and 6.1 ± 0.3 nM for the peptide−RNA complex at 25 °C for the wt and mutant peptide, respectively, suggesting the $\pi-\pi$ interaction between the peptide and RNA contributes only marginally to complex stability (Figure 4). No results were obtained with 5′-(6-Fam)-labeled *boxB* RNA, indicating that the peptides did not directly interact with the fluorescence label. Additionally, a displacement titration resulted in a K_d of 3.8 ± 1.0 nM for unlabeled *boxB* in the wt complex, in the range of the K_d for Nun and the 3′-(6-Fam)-labeled *nutR boxB* RNA (Figure 5).

Structure of the Variant HK022 Nun−boxB Complex. Standard homonuclear two-dimensional NMR experiments (COSY, TOCSY, and NOESY) proved to be sufficient for obtaining sequence-specific resonance assignments for Nun(20−44) Y39A, and several NOESY cross-peaks in the backbone amide−amide region indicating a helical fold for large parts of the peptide could be assigned (Table 3). In particular, for amino acids T23−R29 and I37−L42, helix-typical $i-i+3$ and $i-i+4$ NOEs could be observed, but only very few nonsequential NOEs could be detected from amino acid I30 to R36, indicating structural flexibility in this part of the peptide. For the C- and N-terminal amino acids, no nonsequential NOEs could be detected. The ribose resonances for RNA A9 showed the exceptional downfield shift that was already observed for the wt complexes of HK022 Nun and λ N. Consistent with this feature, the $H1'_i-H6/H8_{i+1}$ NOEs that are typically used for the assignment of the ribose spin system and that of the following base (*36*) are missing between A8 and A9 as well as between A9 and A10. Overall, the chemical shifts of the RNA protons of the mutant complex are very similar to the shifts observed for the wt complexes. For further structure calculations, we used the *nutR boxB* RNA conformation from the N36−*boxB* RNA complex as calculated in ref *13* as a starting point, in analogy to ref *12*.

Thirteen intermolecular NOEs could be identified unambiguously in the NOESY spectra. For the β-protons of S24, NOEs with RNA C2 and C3 were observed. Additionally, NOEs between the side chain protons of R28, C4 H5 and U5 H5, could be assigned, suggesting that the interaction between Nun(20−44) Y39A and *boxB* RNA is restricted to S24, R28, and the stem region of the RNA (Figure 6), in good agreement with the observations for wt Nun(20−44) (*12*) and mutational studies of the λ N peptide (*15, 18*).

A PROCHECK-NMR (*27*) analysis of the Nun Y39A−*boxB* RNA complex shows that 80.0% of the residues of the 20 accepted structures are found in the most favored regions and an additional 19.6% in the allowed regions of the Ramachandran plot (Table 3). For Nun(20−44) Y39A, formation of an α-helix for residues S24−I30 as well as an additional α-helical turn for residues A38−L41 was found, in good agreement with the wt complex structure, in which Nun(20−44) forms a bent α-helix for residues S24−N43, with the kink at A31 and R32. Clearly, the α-helix for Nun(20−44) Y39A from residue S24 to I30 is stabilized by its interaction with *boxB* RNA, and the loss of secondary structure in the carboxyl-terminal part is due to the lack of stabilization by the $\pi-\pi$ interaction between Y39 and RNA A7 that is present in the wt complex. The α-helical turn for residues A38−L41 is independently induced by the helix favoring three alanines and one leucine in this sequence. The

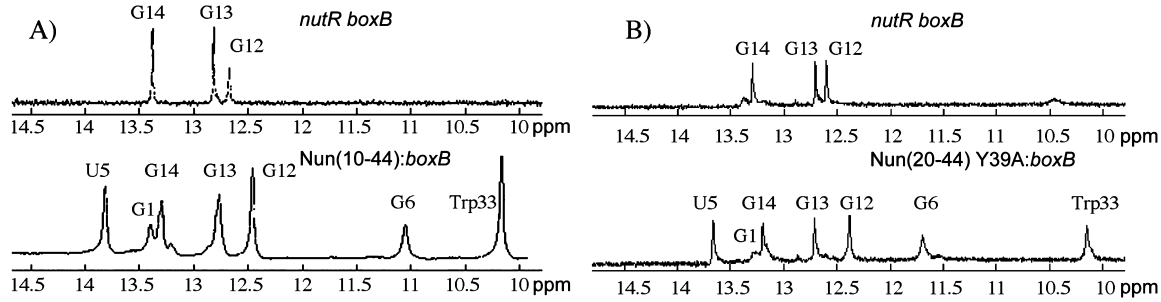

FIGURE 3: (A) One-dimensional NMR spectra of the imino proton region of *nutR boxB* RNA and the Nun(10−44)−*boxB* complex (*11*). (B) One-dimensional NMR spectra of the imino proton region of *nutR boxB* RNA and the Nun(20−44) Y39A−*boxB* complex. All spectra were recorded in a H_2O/D_2O mixture (9:1), 40 mM NaCl, and 50 mM potassium phosphate (pH 6.4) at 298 K.

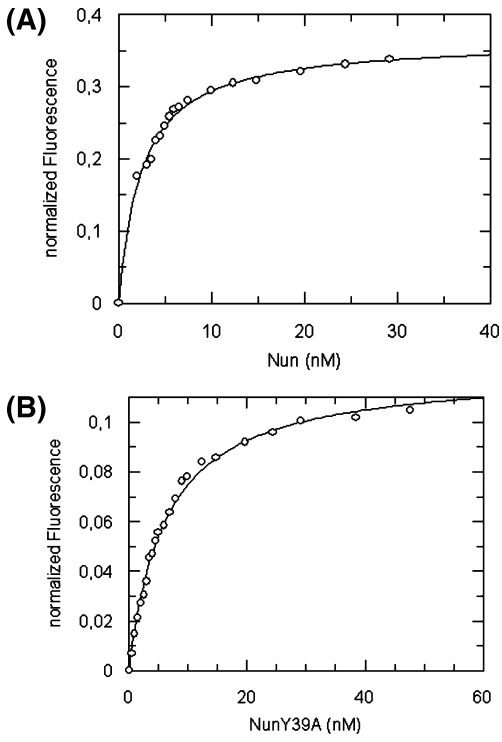

FIGURE 4: Fluorescence equilibrium titrations with (A) Nun and (B) Nun Y39A. 3′-(6-Fam)-labeled *nutR boxB* RNA (50 pM) was titrated with each peptide in 40 mM NaCl and 50 mM potassium phosphate (pH 6.4) at 298 K. The curves show the best fit to eq 1. A K_d value of 2.4 nM was determined for Nun and a K_d value of 6.1 nM for Nun Y39A.

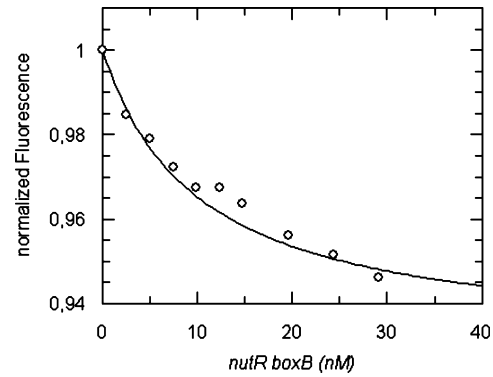

FIGURE 5: Displacement titration of 3′-(6-Fam)-labeled *nutR boxB* RNA with unlabeled *nutR boxB* RNA. Labeled RNA (10 nM) and Nun (10 nM) were titrated with unlabeled RNA in 40 mM NaCl and 50 mM potassium phosphate (pH 6.4) at 298 K. The curve shows the best fit to eq 2. A K_d value of 3.8 nM was determined.

experimental results thus clearly confirm the MD simulations, that is, formation of an α-helix for residues S24−I30 and higher flexibility in the carboxyl-terminal part with a short α-helical turn for residues A38−L41.

Comparison of λ N−boxB and HK022 Nun−boxB Complexes. The conformations of *boxB* RNA complexes of λ N and HK022 Nun ARM peptides are highly similar, and the K_d values for both are in the low nanomolar range as confirmed here [2.4 ± 0.1 and 1.3 ± 0.4 nM (*11*) for Nun and N, respectively]. This difference can be pinpointed to the presence of S23 in Nun at the position equivalent to A3 in λ N; λ N A3S showed a decrease to 80% compared to the wt affinity in gel mobility shift assays (*18*). Thus, A3 is key for the stability of the N ARM peptide−*boxB* complex.

The increase in the K_d for the Nun Y39A−*boxB* complex is negligible, whereas for the N W18A mutant, no RNA binding could be detected in gel shift experiments (*18*). The λ N double mutant E14R15 lacks the W18−A7 interaction and shows only basal antitermination activity (*38*), although the K_d of 7 nM is only slightly increased compared to that of the wt peptide. Thus, the major contributions to the stability of the N−*boxB* complex appear to originate from N A3−RNA stem interaction as well as from W18−A7 stacking; however, the latter interaction also seems to be crucial for functionality. In contrast, the HK022 Nun−*boxB* complex is neither functionally nor energetically dependent on the corresponding stacking interaction. This follows the pattern in which tyrosine stacking was reported to be energetically less favorable than tryptophan stacking (*39*). Thus, weakened stacking interaction and the serine-for-alanine substitution in Nun could explain the slightly higher K_d of the Nun complex, although the extent of the K_d increase seems far too small. Thus, the tyrosine-for-tryptophan and serine-for-alanine substitution must to some extent be offset by other amino acid−base interactions. The availability of an EOP test for Nun mutants and the combination of the test results with MD calculations are expected to shed further light on the details of this peptide−RNA interaction.

Even mutations of amino acids that are involved in binding to the RNA stem region do not lead to a complete loss of Nun termination activity, which, on a functional level, could be explained by the fact that for efficient termination, the Nun−*boxB* complex needs to persist only for the time span needed by the TEC to read through ~100 bp; the λ N−*boxB* complex, however, has to persist for the time span the TEC needs to read through several kilo base pairs. This significant difference could explain the importance of the W18−A7 $\pi-\pi$ interaction with respect to functionality as it may help

Table 3: Structural Statistics

Experimentally Derived Restraints	
no. of distance restraints	
NOEs	202
intraresidual	0
sequential	98
medium-range	91
long-range	0
intermolecular	13
Restraint Violations	
average distance restraint violation	0.0075 ± 0.0024 Å
maximum distance restraint violation	<0.1 Å
Deviation from Ideal Geometry	
bond lengths	0.00225 ± 0.00003 Å
bond angles	0.489 ± 0.003°
Coordinate Precision[a]	
Arg20−Gly44	Ser24−Lys42
backbone heavy atoms, 2.12 Å	backbone heavy atoms, 1.53 Å
all heavy atoms, 3.10 Å	all heavy atoms, 2.57 Å
Arg20−Gly44 + *boxB* RNA	Ser24−Lys42 + *boxB* RNA
backbone heavy atoms, 2.56 Å	backbone heavy atoms, 2.10 Å
all heavy atoms, 3.55 Å	all heavy atoms, 3.07 Å
Ramachandran Plot Statistics[b]	
80.0%, 18.2%, 1.4%, 0.5%	

[a] The precision of the coordinates is defined as the average atomic root-mean-square deviation between the accepted simulated annealing structures and the corresponding mean structure calculated for the given sequence regions. [b] Ramachandran plot statistics are determined by PROCHECK-NMR and given in the following order: most favored, additionally allowed, generously allowed, disallowed.

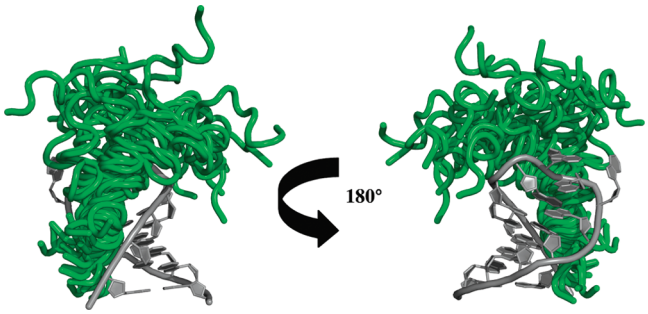

FIGURE 6: Overlay of the 20 lowest-energy structures of the Nun Y39A−*boxB* RNA complex. The peptide structure (green) is well-defined at the RNA (gray) interface but is highly flexible after the bend between amino acids 31 and 33. Both regions of the peptide are helical. Structural calculations were performed with a total number of 189 intramolecular and 13 intermolecular distance restraints. All structures exhibited NOE violations of <0.1 Å.

to add that small amount of binding energy necessary to keep the λ N−*boxB* complex stable long enough for antitermination, but which is not necessary for the short lifetime required for the HK022 Nun−*boxB* complex to exert its activity.

ACKNOWLEDGMENT

We thank Ulrike Persau and Britta Zimmermann for RNA preparations. We thank J. Pan for construction of *pTrc-Nun Y39A* and N. Costantino and D. Court for the *nut-lacZ* fusions.

REFERENCES

1. Robert, J., Sloan, S. B., Weisberg, R. A., Gottesman, M. E., Robledo, R., and Harbrecht, D. (1987) The remarkable specificity of a new transcription termination factor suggests that the mechanisms of termination and antitermination are similar. *Cell 51*, 483–492.
2. Robledo, R., Gottesman, M. E., and Weisberg, R. A. (1990) Lambda nutR mutations convert HK022 Nun protein from a transcription termination factor to a suppressor of termination. *J. Mol. Biol. 212*, 635–643.
3. Das, A. (1993) Control of transcription termination by RNA-binding proteins. *Annu. Rev. Biochem. 62*, 893–930.
4. Greenblatt, J., Nodwell, J. R., and Mason, S. W. (1993) Transcriptional antitermination. *Nature 364*, 401–406.
5. Chattopadhyay, S., Garcia-Mena, J., DeVito, J., Wolska, K., and Das, A. (1995) Bipartite function of a small RNA hairpin in transcription antitermination in bacteriophage lambda. *Proc. Natl. Acad. Sci. U.S.A. 92*, 4061–4065.
6. Oberto, J., Weisberg, R. A., and Gottesman, M. E. (1989) Structure and function of the nun gene and the immunity region of the lambdoid phage HK022. *J. Mol. Biol. 207*, 675–693.
7. Franklin, N. C. (1985) Conservation of genome form but not sequence in the transcription antitermination determinants of bacteriophages λ, φ21 and P22. *J. Mol. Biol. 181*, 75–84.
8. Lazinski, D., Grzadzielska, E., and Das, A. (1989) Sequence-specific recognition of RNA hairpins by bacteriophage antiterminators requires a conserved arginine-rich motif. *Cell 59*, 207–218.
9. Chattopadhyay, S., Hung, S. C., Stuart, A. C., Palmer, A. G., III, Garcia-Mena, J., Das, A., and Gottesman, M. E. (1995) Interaction between the phage HK022 Nun protein and the nut RNA of phage lambda. *Proc. Natl. Acad. Sci. U.S.A. 92*, 12131–12135.
10. Watnick, R. S., Herring, S. C., Palmer, A. G., III, and Gottesman, M. E. (2000) The carboxyl terminus of phage HK022 Nun includes a novel zinc-binding motif and a tryptophan required for transcription termination. *Genes Dev. 14*, 731–739.
11. Van Gilst, M. R., Rees, W. A., Das, A., and von Hippel, P. H. (1997) Complexes of N antitermination protein of phage λ with specific and nonspecific RNA target sites on the nascent transcript. *Biochemistry 36*, 1514–1524.
12. Faber, C., Schärpf, M., Becker, T., Sticht, H., and Rösch, P. (2001) The structure of the coliphage HK022 Nun protein-λ-phage boxB RNA complex. Implications for the mechanism of transcription termination. *J. Biol. Chem. 276*, 32064–32070.
13. Schärpf, M., Sticht, H., Schweimer, K., Boehm, M., Hoffmann, S., and Rösch, P. (2000) Antitermination in bacteriophage λ. The structure of the N36 peptide-boxB RNA complex. *Eur. J. Biochem. 267*, 2397–2408.
14. Legault, P., Li, J., Mogridge, J., Kay, L. E., and Greenblatt, J. (1998) NMR structure of the bacteriophage λ N peptide/boxB RNA complex: Recognition of a GNRA fold by an arginine-rich motif. *Cell 93*, 289–299.
15. Xia, T., Frankel, A., Takahashi, T. T., Ren, J., and Roberts, R. W. (2003) Context and conformation dictate function of a transcription antitermination switch. *Nat. Struct. Biol. 10*, 812–819.
16. Xia, T., Wan, C., Roberts, R. W., and Zewail, A. H. (2005) RNA-protein recognition: Single-residue ultrafast dynamical control of structural specificity and function. *Proc. Natl. Acad. Sci. U.S.A. 102*, 13013–13018.
17. Franklin, N. C. (1993) Clustered arginine residues of bacteriophage λ N protein are essential to antitermination of transcription, but their locale cannot compensate for boxB loop defects. *J. Mol. Biol. 231*, 343–360.
18. Su, L., Radek, J. T., Hallenga, K., Hermanto, P., Chan, G., Labeots, L. A., and Weiss, M. A. (1997) RNA recognition by a bent α helix regulates transcriptional antitermination in phage λ. *Biochemistry 36*, 12722–12732.
19. Müller, B., Restle, T., Reinstein, J., and Goody, R. S. (1991) Interaction of fluorescently labeled dideoxynucleotides with HIV-1 reverse transcriptase. *Biochemistry 30*, 3709–3715.
20. Cavanagh, J., Fairbrother, W. J., Palmer, A. G., III, Rance, M., and Skelton, N. J. (2006) *Protein NMR spectroscopy: principles and practice*, Academic Press, San Diego.
21. Johnson, B. A., and Blevins, R. A. (1994) NMRView: A computer program for the visualization and analysis of NMR data. *J. Biomol. NMR 4*, 603–614.
22. Schwieters, C. D., Kuszewski, J. J., and Clore, G. M. (2006) Using Xplor-NIH for NMR molecular structure determination. *Prog. Nucl. Magn. Reson. Spectrosc. 48*, 47–62.
23. Schwieters, C. D., Kuszewski, J. J., Tjandra, N., and Clore, G. M. (2003) The Xplor-NIH NMR Molecular Structure Determination Package. *J. Magn. Reson. 160*, 66–74.

24. Nilges, M., Clore, G. M., and Gronenborn, A. M. (1988) Determination of three-dimensional structures of proteins from interproton distance data by dynamical simulated annealing from a random array of atoms. *FEBS Lett. 239*, 129–136.
25. Holak, T. A., Nilges, M., and Oschkinat, H. (1989) Improved strategies for the determination of protein structures from NMR data: The solution structure of acyl carrier protein. *FEBS Lett. 242*, 218–224.
26. Kuszewski, J., Gronenborn, A. M., and Clore, G. M. (1996) Improving the quality of NMR and crystallographic protein structures by means of a conformational database potential derived from structure databases. *Protein Sci. 5*, 1067–1080.
27. Laskowski, R. A., Rullmannn, J. A., MacArthur, M. W., Kaptein, R., and Thornton, J. M. (1996) AQUA and PROCHECK-NMR: Programs for checking the quality of protein structures solved by NMR. *J. Biomol. NMR 8*, 477–486.
28. DeLano, W. L. (2002) *PyMOL*, DeLano Scientific, Palo Alto, CA.
29. Wilson, H. R., Kameyama, L., Zhou, J. G., Guarneros, G., and Court, D. L. (1997) Translational repression by a transcriptional elongation factor. *Genes Dev. 11*, 2204–2213.
30. Miller, J. H. (1992) *A Short Course in Bacterial Genetics: A Laboratory Manual for Escherichia coli and Related Bacteria*, Cold Spring Harbor Laboratory Press, Plainview, NY.
31. Kim, H. C., Washburn, R. S., and Gottesman, M. E. (2006) Role of *E. coli* NusA in phage HK022 Nun-mediated transcription termination. *J. Mol. Biol. 359*, 10–21.
32. Case, D. A., Darden, T. A., Cheatham, T. E., Simmerling, C. L., Wang, J., Duke, R. E., Luo, R., Merz, K. M., Pearlman, D. A., Crowley, M., Walker, R. C., Zhang, W., Wang, B., Hayik, S., Roitberg, A., Seabra, G., Wong, K. F., Paesani, F., Wu, X., Brozell, S., Tsui, V., Gohlke, H., Yang, L., Tan, C., Mongan, J., Hornak, V., Cui, G., Beroza, P., Mathews, D. H., Schafmeister, C., Ross, W. S., and Kollman, P. A. (2006) *Amber 9*, University of California, San Francisco.
33. Duan, Y., Wu, C., Chowdhury, S., Lee, M. C., Xiong, G., Zhang, W., Yang, R., Cieplak, P., Luo, R., Lee, T., Caldwell, J., Wang, J., and Kollman, P. (2003) A point-charge force field for molecular mechanics simulations of proteins based on condensed-phase quantum mechanical calculations. *J. Comput. Chem. 24*, 1999–2012.
34. Lee, M. C., and Duan, Y. (2004) Distinguish protein decoys by using a scoring function based on a new AMBER force field, short molecular dynamics simulations, and the generalized born solvent model. *Proteins 55*, 620–634.
35. Price, D. J., and Brooks, C. L., III (2004) A modified TIP3P water potential for simulation with Ewald summation. *J. Chem. Phys. 121*, 10096–10103.
36. Johnson, N. P., Baase, W. A., and von Hippel, P. H. (2005) Low energy CD of RNA hairpin unveils a loop conformation required for λN antitermination activity. *J. Biol. Chem. 280*, 32177–32183.
37. Varani, G., and Tinoco, I., Jr. (1991) RNA structure and NMR spectroscopy. *Q. Rev. Biophys. 24*, 479–532.
38. Xia, T., Becker, H. C., Wan, C., Frankel, A., Roberts, R. W., and Zewail, A. H. (2003) The RNA-protein complex: Direct probing of the interfacial recognition dynamics and its correlation with biological functions. *Proc. Natl. Acad. Sci. U.S.A. 100*, 8119–8123.
39. Kobayashi, H., Kato, J., Morioka, H., Stewart, J. D., and Ohtsuka, E. (1999) Tryptophan H33 plays an important role in pyrimidine (6−4) pyrimidone photoproduct binding by a high-affinity antibody. *Protein Eng. 12*, 879–884.

BI8004347